Nanocrystal Surface Structure Analysis by Analytical Ultracentrifugation

Helmut Cölfen,*,† Shay Tirosh,‡ and Arie Zaban‡

Max-Planck-Institute of Colloids and Interfaces, Colloid Chemistry, Research Campus Golm, Am Mühlenberg, 14476 Golm, Germany, and Chemistry Department, Bar Ilan University, Ramat-Gan, 52900, Israel

Received April 25, 2003. In Final Form: October 8, 2003

Sedimentation velocity experiments on two TiO_2 model colloids with similar properties but different surface structures were performed as a function of the solution pH in order to differentiate between similar size particles. The particle sedimentation velocity is highly sensitive to the surface structure, which is indicative of the exposed crystal face of the nanocrystals. Increase of the pH from 1 to 3 resulted in aggregation of all particles in one sample, whereas only partial aggregation occurred for the other, although the ζ-potential of both samples is almost identical in that pH range indicating particle stability. Although the particles are not distinguishable by the conventional methods for particle charge determination, they are clearly different in terms of their sedimentation coefficient distributions. Furthermore, analytical ultracentrifugation (AUC) reveals a dependence of the onset of large aggregate formation on the particle surface. This suggests that AUC has the potential to quantitatively determine differences in the particle surface structure even for polydisperse samples with constant average charge where conventional ζ-potential measurements yield only a constant average value. As ultracentrifugation yields distributions, we further discuss whether a combination with a second independent method like flow-field-flow fractionation can yield particle size and charge distributions in a global analysis approach.

Introduction

The research, development, and use of nanosize materials have increased in recent years as part of the dramatic growth of nanotechnology. The literature provides numerous applications in which the special size-induced properties of nanoparticles are utilized.[1−3] Both the perfection of existing applications and the design of new systems benefit from the ability to tune properties, such as the spectral response, energy levels, and electronic structure, via control of the material size.[1−3] However, the most fundamental characteristic of nanoparticles is their high surface-to-volume ratio, which turns any application consisting of nanoparticles into a high surface area system. The exposed surfaces of crystalline particles depend on the crystal structure and the cleaving orientation.[3−5] From bulk crystals, we know that the properties of the different surface structures vary significantly.[3] Thus, two nanocrystals that are considered similar in terms of size, size distribution, shape, and crystal structure may perform considerably differently only because their surface structures are different.[4−7]

For example, we found that the surface affects the stability and the photoelectrochemical activity of nanosize TiO_2.[8] The transformation temperature from anatase to the more stable structure, the rutile, was altered by more than 150 °C, and the performance of dye-sensitized solar cells consisting of these particles improved, only due to surface effects on the nanoparticles.[8] In the above study, the surfaces of the nanoparticles were examined by dark field transmission electron microscopy (TEM) giving the relative fraction of crystals exposing the 101 face. It was found to be 3 times larger in one sample compared to the other, indicating a significantly different exposed surface. Thus, regardless of the specific size-induced property that prompts the use of nanosize materials in a particular application, surface effects can become a significant factor in the overall performance of this application. When surface-related processes are associated with the nanomaterial utilization, like in many catalysis or electrochemical applications,[2,4,7] the specific surface properties of these particles become crucial. Therefore it is important to develop the ability to characterize the surface of nanoparticles in addition to the standard parameters such as size, size distribution, shape, and crystal structure, that are usually considered.

Currently the ability to determine the surface structures of nanoparticles is usually limited to techniques that lack a statistical significance like electron microscopy and scanning probe techniques or to macroscopic measurements adopted from bulk systems that average the overall surface characteristics.[3,4] The natural, more or less pronounced, polydispersity of inorganic nanoparticles leads to a superposition of the surface properties with the particle size distribution and is thus very difficult to address. Analytical ultracentrifugation (AUC, for a recent review see ref 9) is known as a superior technique which

* To whom correspondence should be addressed. E-mail: coelfen@mpikg-golm.mpg.de.

† Max-Planck-Institute of Colloids and Interfaces.

‡ Bar Ilan University.

(1) *Nanoscale Materials in Chemistry*; Klabunde, K. J., Ed.; John Wiley & Sons: New York, 2001.

(2) *Nanocrystalline Metals and Oxides, Selected Properties and Applications*; Knauth, P., Schoonman, J., Eds.; Kluwer Academic: New York, 2001.

(3) *Hand Book of Nanostructured Materials and Nanotechnology*; Nalwa, H. S., Ed.; Academic Press: San Diego, 2001.

(4) Shklover, V.; Nazeeruddin, M. K.; Zakeeruddin, S. M.; Barbe, C.; Kay, A.; Haibach, T.; Steurer, W.; Hermann, R.; Nissen, H. U.; Grätzel, M. *Chem. Mater.* **1997**, *9*, 430.

(5) Oliver, P. M.; Watson, G. W.; Kelsey, E. T.; Parker, S. C. *J. Mater. Chem.* **1997**, *7*, 563.

(6) Penn, R. L.; Banfield, J. F. *Am. Mineral.* **1998**, *83*, 1077.

(7) Kato, K.; Torii, Y.; Taoda, H.; Kato, T.; Butsugan, Y.; Niihara, K. *J. Mater. Sci. Lett.* **1996**, *15*, 913−915.

(8) Zaban, A.; Aruna, S. T.; Tirosh, S.; Gregg, B. A.; Mastai, Y. *J. Phys. Chem. B* **2000**, *104*, 4130.

10.1021/la0347051 CCC: $25.00
Published on Web 11/19/2003

can deal very well with polydispersity as it can fractionate a sample according to size and density over the entire colloidal range with high statistical significance as every particle is detected.[10,11] AUC can in certain circumstances even determine the particle size distributions of the smallest colloids, <1 nm, with angstrom resolution.[12] This resolution includes subcritical soluble complexes, if present,[13] and the possibility to visualize small changes in the apparent particle size distribution caused by a slightly altered chemical structure of dispersant molecules.[14] As particle sedimentation is also dependent on particle shape[15] and charge[16] (primary and secondary charge effects, sedimentation potential/Dorn effect[17]), it should be possible to determine the influence of particle surface properties, such as charge, chemical surface structure, hydration, and so forth, via the sedimentation coefficient, even for polydisperse particles if the particle shape and density remain constant.

We report here on the application of AUC for surface characterization of nanosize crystals. As a model system, we utilized two TiO_2 nanocrystal suspensions that have a similar size (18 nm diameter), size distribution, and crystal structure (anatase) but differ by their surface structure distributions. We show that AUC is a sensitive tool for differentiating between the particles with respect to the particle surface as well as their aggregation state, even if their ζ-potentials are similar in the investigated pH range. To the best of our knowledge, this is the first time that analytical ultracentrifugation is used to investigate surface properties of particles.

Experimental Section

Colloid Synthesis. Two sets of TiO_2 colloids were prepared using the standard hydrothermal method reported previously.[8] This method includes titration of titanium isopropoxide into acid followed by aging and hydrothermal treatment. The major difference between the two preparations relates to the type of acid used: nitric acid in one case and acetic acid in the other. To achieve the same crystal size in both preparations, small changes in the pH and the autoclaving temperature were performed.

Two aliquots of 11.5 mL of titanium(IV) isopropoxide (Ti[OCH-$(CH_3)_2]_4$, Aldrich, 99.9%) in 11.5 mL of dry 2-propanol were added into vigorously stirred 15.4 mL solutions of pH 2 acetic acid (sample 1) and pH 1.9 nitric acid (sample 2). The solutions were subjected to aging at ambient temperature for 12 h followed by heating to 82 °C for 2 h to evaporate the 2-propanol. Finally the two solutions were transferred to titanium autoclaves (Parr Instrument) for a hydrothermal treatment at 250 °C (nitric acid solution) and 280 °C (acetic acid solution) for 13 h. For characterization of the colloids in the ultracentrifuge, they were transferred to 0.1 N HNO_3 (pH 1). The transfer process included extensive washing cycles with basic water and finally nitric acid to ensure similar starting points and rule out possible chemisorption of carboxylic acids.[18]

Colloid Characterization. X-ray diffraction patterns were used to determine the identity, quantity, and crystallite size of each phase present. The powder X-ray diffraction (XRD) patterns were recorded using an X-ray diffractometer (Rigaku 2028) with Cu Kα radiation. The average crystallite size, d, of the hydrothermally prepared powders was calculated from the Scherrer formula.[19] TEM imaging was carried out with a JEOL microscope, operating at 100 kV. Samples for TEM analysis were prepared by dispersing TiO_2 onto TEM copper grids coated with thin amorphous carbon. ζ-Potentials were measured with a Malvern Zetasizer (Malvern Instruments). Dynamic light scattering at a 90° angle was performed on a NICOMP submicron particle sizer model 370 (NICOMP, Santa Barbara, CA).

Sedimentation velocity experiments were performed at 25 °C on an Optima XL-I ultracentrifuge (Beckman-Coulter, Palo Alto, CA) equipped with an on-line Rayleigh interference and scanning UV−vis absorption optics (200−800 nm) at 5000 rpm. Twelve millimeter charcoal-filled Epon centerpieces were used due to the extremely low applied pH. The investigated solutions were initially in 0.1 N HNO_3 ($\rho = 1.000\ 48$ g/mL and $\eta = 0.891\ 97$ cP at 25 °C) and were pH adjusted with NaOH. To avoid extrapolations of concentration series, the concentrations were chosen to be very low, between 0.09 and 0.41 mg/mL, which are normally considered close to ideal dilution (1.8−8.5 interference fringes, solution concentrations calculated via dn/dc of anatase = 1.1675 mL/g using $n_{water} = 1.3325$ and $n_{Anatase} = 2.5$ at 25 °C). The sedimentation velocity experiments were evaluated with the least-squares g(s*) method in the SEDFIT software by P. Schuck,[20] which yields sedimentation coefficient distributions not corrected for diffusion broadening.

Results and Discussion

Figure 1 presents TEM pictures of the two nanosize TiO_2 suspensions that are compared in this work. The particles have the shapes that are typical of irregular nanocrystals with rounded edges. Counting 140 particles for each sample, we find the number-average size to be 18.7 nm for sample 1 and 17.2 nm for sample 2 with the respective standard deviations of 6.5 and 4.2 nm. These evaluations were repeated for three additional areas on the TEM grid to ensure that the given particle sizes are representative. Figure 2 shows the X-ray diffractograms of the two samples indicating the anatase for both cases. The volume-average crystallite sizes calculated from the [101] peak broadening of the diffractograms are 18.7 nm for sample 1 and 16.7 nm for sample 2, which are slightly lower than expected when compared with the microscopy number averages. This may be due to the different crystal growth orientation of the two samples with respect to the [101] face but is still well within the error limits. In other words, the two colloid batches are quite similar in size, size distribution, crystal structure, and shape.

While the standard characterization discussed above shows that the two colloid batches are very similar in their properties, it provides no information regarding their surface. As an indirect indicator of the surface charge, ζ-potential measurements can be employed, which show that the particles are also very similar with respect to their charge (Figure 3). Only at pH values above the isoelectric point do differences between the samples become obvious.

To further characterize the particle surface, we performed sedimentation velocity experiments to determine the sedimentation coefficient distributions of the two

(9) Cölfen, H. Analytical Ultracentrifugation of Nanoparticles. In *Encyclopedia of Nanoscience and Nanotechnology*; Nalwa, H. S., Ed.; American Scientific Publishers: Stevenson Ranch, CA, 2004; in press.

(10) Mächtle, W. Analysis of polymer dispersions with an eight cell AUC multiplexer: High-resolution particle size distribution and density gradient techniques. In *Analytical Ultracentrifugation in Biochemistry and Polymer Science*; Harding, S. E., Rowe, A. J., Horton, J. C., Eds.; The Royal Society of Chemistry: Cambridge, 1992; p 147.

(11) Müller, H. G. *Colloid Polym. Sci.* **1989**, *267*, 1113.

(12) Cölfen, H.; Pauck, T. *Colloid Polym. Sci.* **1997**, *275*, 175.

(13) Cölfen, H.; Schnablegger, H.; Fischer, A.; Jentoft, F. C.; Weinberg, G.; Schlögl, R. *Langmuir* **2002**, *18*, 3500.

(14) Börger, L.; Cölfen, H.; Antonietti, M. *Colloids Surf., A* **2000**, *163*, 29.

(15) Harding, S. E. *Biophys. Chem.* **1995**, *55*, 69.

(16) Schachman, H. K. *Ultracentrifugation in Biochemistry*; Academic Press: New York, 1959. Pedersen, K. O. *Z. Phys. Chem.* **1934**, *A170*, 41.

(17) Ohshima, H.; Healy, T. W.; White, L. R.; O'Brien, R. W. *J. Chem. Soc., Faraday Trans. 2* **1984**, *80*, 1299.

(18) Schmidt, H.; Nass, M.; Aslan, M.; Schmitt, K.-P.; Benthien, T.; Albayrak, S. *J. Phys. IV, Colloque C7, supplement au J. Phys. III* **1993**, *3*, 1251.

(19) West, A. R. In *Solid State Chemistry and its Applications*; John Wiley & Sons: Singapore, 1987; p 173.

(20) Schuck, P. *Biophys. J.* **2000**, *78*, 1606.

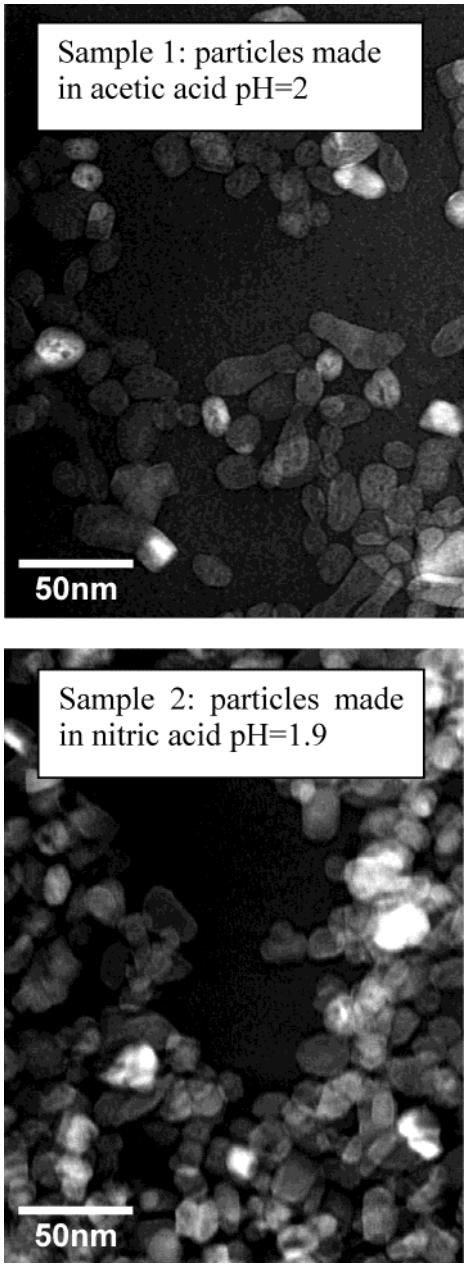

Figure 1. TEM pictures of the two nanosize TiO_2 samples compared in this work showing an average crystallite size of 18.7 nm (standard deviation, 6.5) for sample 1 and 17.2 nm (standard deviation, 4.2) for sample 2.

samples. The sedimentation coefficient distribution depends on particle size (including hydration water), density (including hydration water), shape, and charge of the particles. While the dependence of the sedimentation coefficient on the first three properties, that is, particle size, density, and shape, is rather intuitive, the surface charge effect requires some elaboration. The surface charges influence the sedimentation via two processes: (1) the primary charge effect and (2) particle aggregation. For a salt-free solution of the charged particles, the sedimentation coefficient is much lower and the diffusion coefficient much higher than that of a similar uncharged particle. This is called the primary charge effect and is attributed to the electric field which is generated when a sedimenting charged particle is separated from its slowly sedimenting counterions.[16,21] In other words, the counterions decelerate the particle sedimentation velocity, which is evident in the decreased sedimentation coefficient and the formation of a sedimentation potential.[17] The second process involves the change of sedimentation coefficient due to particle aggregation. However, colloidal stabilization/aggregation may be affected by further effects including repulsive hydration forces, which occur at $I > 0.02$ and may lead to dispersion of rutile TiO_2 even at its isoelectric point of pH $\approx$ 6.2 at 1 M NaCl.[22]

In other words, the AUC measurement that provides a distribution of sedimentation coefficients is highly sensitive to aggregation including small aggregates in small amounts. The effect is evident in the increase of the sedimentation coefficient and a change of the distribution shape. Thus comparing the sedimentation coefficient distribution of samples 1 and 2, which have a quite similar particle size, density, and shape, should correlate to the particle surface, which is highly affected by the crystal face exposed by the nanocrystals as well as so called "structural forces", for example, the correlated local changes of the surface-bound water structure under the influence of the force fields originating from the exposed crystal faces.[23]

Figure 4 shows the sedimentation coefficient distributions of the two samples as a function of the solution pH

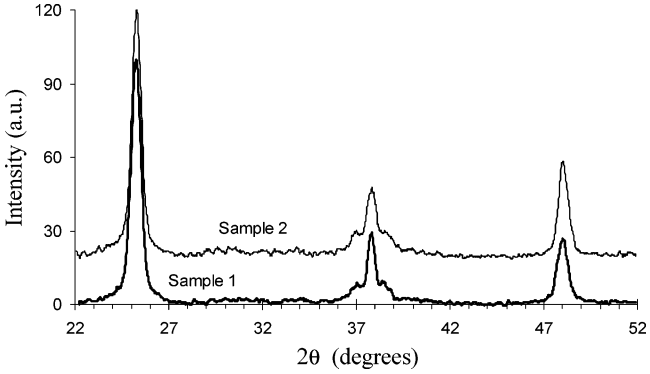

Figure 2. X-ray diffractograms of the two samples compared in this work indicating that both samples consist of anatase crystals. Volume-average grain sizes of 18.7 nm for sample 1 and 16.7 nm for sample 2 were calculated from the peak broadening of the diffractograms.

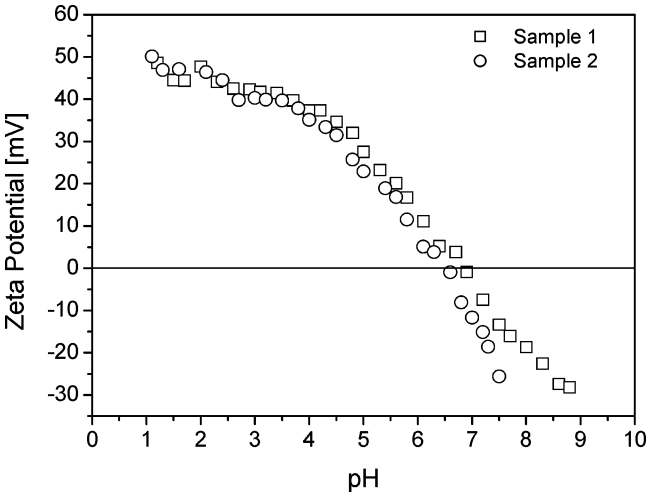

Figure 3. pH dependence of the ζ-potential for samples 1 and 2.

(21) Pedersen, K. O. *Z. Phys. Chem.* **1934**, *A170*, 41.

(22) Yotsumotu, H.; Yoon, R. H. *J. Colloid Interface Sci.* **1993**, *157*, 426.

(23) Churaev, N. V.; Derjaguin, B. V. *J. Colloid Interface Sci.* **1985**, *103*, 542.

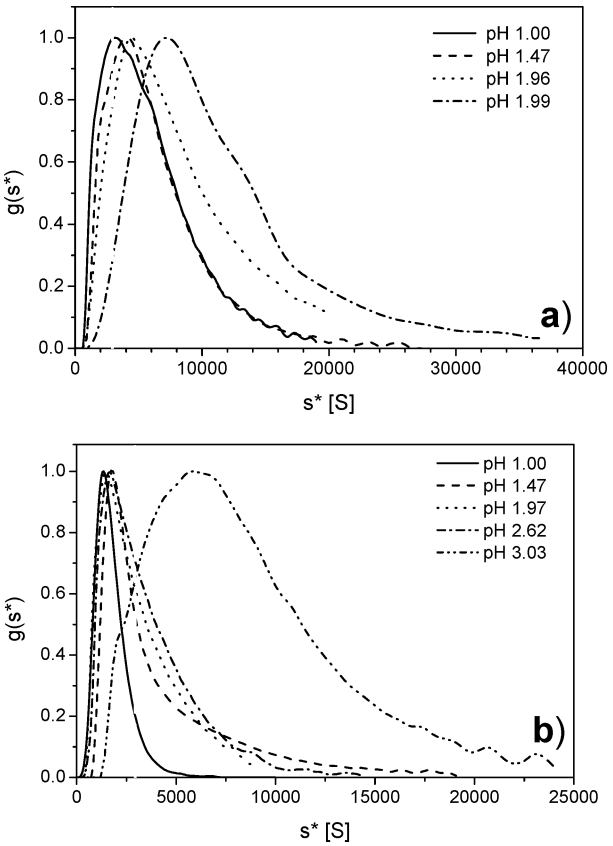

Figure 4. pH-dependent sedimentation coefficient distributions for (a) sample 2 and (b) sample 1.

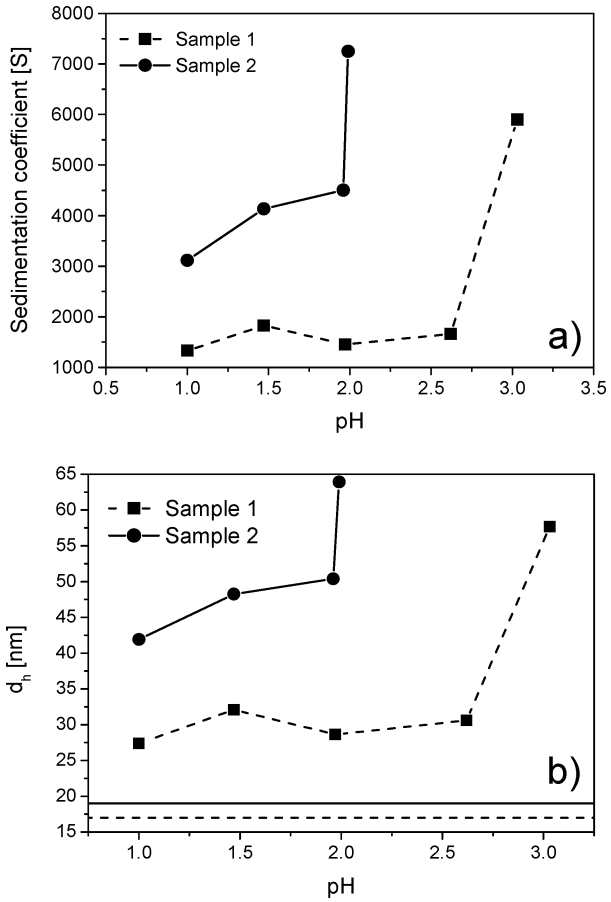

Figure 5. (a) Sedimentation coefficients from the peak maximum of the sedimentation coefficient distribution at different solution pHs; (b) pH-dependent particle sizes calculated on the basis of the sedimentation coefficients presented in part a with a bulk anatase density of 3.84 g/mL. The horizontal lines in part b indicate the particle diameters from electron microscopy and XRD (see above).

starting at a low pH value. The sedimentation coefficient distributions were not corrected for the effects of diffusion broadening so that they appear broader than the real distribution.

Figure 4 clearly shows that the sedimentation coefficient distributions of the two tested samples are not the same. They differ by the peak maximum, width, shape, and response to the solution pH. In the following section, we show that this behavior results from the different surfaces of the two nanocrystal samples expressed by the process of particle aggregation. With respect to other methods that provide an average charge value (like ζ-potential measurements), the AUC measurement has the advantage of yielding a high-resolution distribution.

Figure 5 presents the peak maximum of the sedimentation coefficient distribution of the two nanocrystal samples at different solution pHs. Starting at pH 1, the sedimentation coefficients at peak maximum (sample 1, 1330 S; sample 2, 3120 S) differ by more than a factor of 2. Both the primary charge effect and the aggregation effect follow the same trend for a decreased electrostatic particle stabilization due to an increase in the ionic strength. As the particles appear to be similarly charged according to the ζ-potential measurements (Figure 3), the huge observed differences are a reflection of the differing particle surface structures expressed in their aggregation behavior. From Figure 5b and the comparison with the primary particle sizes (solid horizontal lines), it becomes clear that already at pH 1 the particles are aggregated, either during synthesis or washing, although to a different extent. Again, this can be attributed to a different particle surface structure of the two samples.

When we increase the pH by base addition, the ionic strength of 0.1 mol/L, which is determined by the high nitric acid concentration, is not notably changed. Thus it cannot be argued that the particle charge is screened more and more by the increase in the counterion concentration providing a lower electrostatic contribution toward electrostatic stabilization due to the decrease in the electric double layer upon the approach to the point of zero charge, pH 6.9 for sample 1 and pH 6.6 for sample 2 (ζ-potential measurements, Figure 3, above). Consequently, when purely considering the simple Derjaguin−Landau−Verwey−Overbeek (DLVO) theory (van der Waals attraction and electrostatic repulsion) for electrostatically stabilized colloids, with increasing pH and in the absence of aggregation, the *s*-value should be constant up to the point where the colloids undergo massive aggregation resulting in a sudden rise of the sedimentation coefficient due to chemical changes in the particle surface structure. Figure 5 shows this trend only for sample 1 in a limited pH interval revealing a pronounced difference in the surface structures of the two colloid samples. The *s*-value of sample 2 continuously increases with increasing pH, reaching the significant aggregation at a pH between 1.96 and 1.99. Thus, AUC clearly shows delicate differences between the two preparations, which are all related to the particle surface structure and are expressed in the following: differences in the colloidal stability; subtle charge differences, not being expressed in the ζ-potential; shape of the aggregates; particle hydration.

The observed changes in the sedimentation coefficient may be attributed to differences in the colloidal stability of the two samples, which despite their similar primary

particle size, shape, and density expose different surface structures. The resulting differences in the particle aggregation are also reflected in the volume weighed average hydrodynamic particle diameters d_h and the translational diffusion coefficients D calculated from dynamic light scattering (DLS):

Sample 1 (volume weighed)

pH 1.00 $D = 4.98 \times 10^{-8}$ cm^2/s
$d_h = 64.0 \pm 25.1$ nm

Sample 2 (volume weighed)

pH 1.00 $D = 3.68 \times 10^{-8}$ cm^2/s
$d_h = 87.4 \pm 35.6$ nm

pH 1.47 $D = 2.25 \times 10^{-8}$ cm^2/s
$d_h = 105.7 \pm 66.0$ nm

pH 1.96 $D = 1.99 \times 10^{-8}$ cm^2/s
$d_h = 162.4 \pm 93.8$ nm

The DLS results clearly show that already at pH 1, both samples are aggregated and the polydispersity is rather high. However, the particle sizes from DLS are much larger than those calculated with a bulk anatase density in Figure 5b, but the trend for pH-induced aggregation for sample 2 shown in Figure 5a,b is confirmed. However, this result implies that the nanoparticles have a lower density than assumed in Figure 5b for the bulk anatase particles according to their hydration water, which contributes to the particle sedimentation velocity measured by AUC.

To investigate the pH-dependent particle aggregation in more detail, we have calculated the interaction energies between the particles of radius r applying the DLVO theory. The energy of the attractive van der Waals W_{vdW} interaction was calculated according to[24,25]

$$W_{vdW} = -\frac{A_H}{6}\left(\frac{2}{s^2-4} + \frac{2}{s^2} + \ln\frac{s^2-4}{s^2}\right) \quad (1)$$

with A_H = Hamaker constant, $s = H/r + 2$, r = particle radius, and H = distance between the particles. The Hamaker constant was taken as 26×10^{-20} J for rutile in water,[26] assuming a similar value for anatase. The repulsive electrostatic interaction W_{el} was calculated according to[25]

$$W_{el} = \frac{r}{v^2}\frac{32\pi\epsilon\epsilon_0(RT)^2}{F^2}\gamma^2 e^{-\kappa H} \quad (2)$$

with $\gamma = (e^{z/2} - 1)/(e^{z/2} + 1)$ and $z = vF\psi_0/RT$, v = number of charges per ion, F = Faraday constant, ψ_0 = surface potential at infinite particle distance, R = gas constant, T = absolute temperature, ϵ = relative dielectric constant of the dispersion medium, ϵ_0 = electric field constant, and the Debye length $\kappa = [2IF^2/(\epsilon\epsilon_0 RT)]^{1/2}$ where I is the ionic strength of 0.1 mol/L generated by the extreme pH values. The increase in the ionic strength by pH adjustment could be neglected as it is in the order of 10^{-11}–10^{-13} mol/L. As a limiting case, the unknown surface potential was calculated from the assumption that the potential at the limit of the Stern layer (2 water layers, 0.5 nm) is the ζ-potential. The potential ψ in the distance x of a plane surface can be approximated by

$$\psi = \psi_0 e^{-\kappa x} = B\psi_0 \quad (3)$$

which is similar to the Debye–Hückel approximation for spherical particles for low potentials (<25 mV), where the right-hand side of eq 3 is extended by the factor $r/(r + x)$. For the applied high ionic strengths of $I = 0.1$ mol/L, the surface potential ψ_0 was thus approximated to be at least bigger by a factor B of 1.7 than the ζ-potential.

The DLVO calculations reveal already at pH 1 only an overall attractive interaction without repulsive barrier for $B = 1.7$. Increasing the pH by neutralization does not alter the ionic strength so that attractive interactions result for all pH values.

One further question arises, how can the discrepancies between the AUC results based on the bulk anatase particle density and the DLS results be explained? As both AUC and DLS determine the particle size (including bound water), which can be converted to the average particle density, the average particle density including the hydration water can be expressed by a simple transformation of the Svedberg formula using the d_h values obtained from DLS and assuming the particles to be hard spheres:

$$\rho_p = \frac{18\eta s}{d_h^2} + \rho_s \quad (4)$$

with ρ = density with index p = particle and s = solvent, η = solvent viscosity, d_h = hydrodynamic particle diameter, and s = sedimentation coefficient.

Converting Figure 5a to densities with the particle diameters from DLS and assuming that the particle charge contribution is negligible due to the very low solution concentrations and high ionic strength, respectively, and is constant for both samples, an apparent particle density much lower than that of bulk anatase is obtained. These are ρ_p-values of 1.52 g/mL (sample 1, pH 1), 1.65 g/mL (pH 1, sample 2), 1.59 g/mL (pH 1.47, sample 2), and 1.27 g/mL (pH 1.96, sample 2). According to the above DLVO calculations, no electrostatic repulsive barrier exists so that the particle charge can be treated as sufficiently screened at ionic strengths of ≥0.1 mol/L with respect to the primary charge effect. Thus, even subtle charge changes, not reflected in the ζ-potential, can be ruled out as a reason for the different observed particle sedimentation behavior. Under this condition, the above calculated density appears realistic for the overall particle including the hydration layer provided that the shape of the particles of both samples is spherical. Applying a simple geometrical model of a spherical core (anatase)–shell (hydration layer) particle and the relation $1/\rho_{average} = w_1/\rho_1 + w_2/\rho_2$ with w = mass fraction of components 1 and 2 and assuming the density of the hydration layer to be increased by 10% with respect to free water in coincidence with experimental findings for proteins,[27,28] we obtain the following results: $d_{core} = 46.6$ nm, $\delta_{hydr} = 8.7$ nm (sample 1, pH 1); $d_{core} = 67.8$ nm, $\delta_{hydr} = 9.8$ nm (sample 2, pH 1); $d_{core} = 81.1$ nm, $\delta_{hydr} = 12.3$ nm (sample 2, pH 1.47); and $d_{core} = 101.4$ nm, $\delta_{hydr} = 30.5$ nm (sample 1, pH 1.96). Although the simple core–shell model is certainly not right for the aggregates,

(24) Hamaker, H. C. *Physica 4* **1937**, 1058.
(25) Verwey, E. J. W.; Overbeek, J. T. G. *Theory of the stability of lyophobic colloids. The interactions of sol particles having an electrical double layer*; Elsevier: New York, 1948.
(26) Israelachvili, T. N. *Intermolecular and surface forces*; Academic Press: London, 1994.
(27) Ebel, C.; Eisenberg, H.; Ghirlando, R. *Biophys. J.* **2000**, *78*, 385.
(28) Svergun, D. I.; Richard, S.; Koch, M. H. J.; Sayers, Z.; Kuprin, S.; Zaccai, G. *Proc. Natl. Acad. Sci. U.S.A.* **1998**, *95*, 2267.

these results would mean that a significant amount of hydration water is included within the aggregates, which is visualized by the above hypothetical hydration water shell thicknesses up to 30 nm. Two main conclusions could be drawn from the above results: (a) sample 2 is more hydrated than sample 1 and (b) the hydration increases with increasing pH (sample 2), likely due to the additional inclusion of water between the aggregated particles. However, the above considerations are based on the assumption of a constant shape, which may not be fulfilled for the aggregates so that one runs into the so-called hydration problem,[29] where the shape and the amount of hydration water cannot be determined by AUC alone. A solution of this problem would be a combination of various hydrodynamic techniques to determine hydration-independent shape functions, which is already described for polymers.[15] Thus, global analysis approaches will be of benefit in the future.

In a previous study, we showed the effect of the synthesis medium on the crystal face exposed by the resulting nanocrystals.[8] The above interpretation of the results presented in Figures 4 and 5 is based on this understanding, that is, the primary particle size, size distribution, ζ-potential, and crystal structure are similar in both samples, which only differ in their crystal face distribution. Nevertheless, the particle sedimentation behavior is significantly different, which shows the power of AUC in nanoparticle characterization with respect to particle aggregation and the role of hydration water and aggregate shape caused by variations in the particle surface structure.

Conclusion

We were able to show that it is possible to distinguish between differences in the surface structure of nanoparticles with sedimentation analysis in AUC with high sensitivity. Already the analysis of average sedimentation coefficients can indicate distinct differences between the two TiO_2 model colloids with similar properties except the particle surfaces. However, a much more detailed view is obtained by analysis of the sedimentation coefficient distributions which reveal a different extent of pH-dependent aggregation for the two samples with different particle surfaces. The possibility to determine distributions indicates the potential that sedimentation methods may have in the future to quantitatively address surface properties of nanoparticles. Properties such as particle charge distributions can then possibly be evaluated by theoretical approaches such as that of Stigter, which was developed for the sedimentation of highly charged colloidal spheres.[30] However, a significant drawback at the moment is the superposition of the polydispersity in nanoparticle size, charge, and hydration which cannot be unravelled by means of sedimentation experiments alone, as the reference state of uncharged and unhydrated particles is not available due to their aggregation upon charge neutralization. A similar problem applies for electrophoresis methods where the particle mobility is determined by charge and size. Flow-field-flow fractionation (Fl-FFF) on the other hand is able to work in a far lower concentration regime than AUC thus minimizing the particle−particle interactions with an additional possibility of fraction collection for further analyses[31] so that a particle size distribution may be available free from charge effects. The elimination of nonideality effects due to the far lower analyte concentration compared to AUC was already reported for molar masses derived by gel permeation chromatography.[32] If this is also possible with Fl-FFF, combination of the Fl-FFF data with the sedimentation coefficient distribution and measurements of the average particle charge could yield the surface charge and hydration effects in dependence on the particle size, provided that the particle shape does not differ too much. A similar example of a global analysis was already recently reported for the combination of Fl-FFF and AUC to yield composition information for a multimodal ferritin organic−inorganic hybrid colloid.[33]

Charged systems notoriously represent an obstacle for AUC investigations of polymers, which researchers try to circumvent by application of buffers as solvents. This presents on one hand an obstacle for nanoparticle systems, as they will aggregate upon ionic strength increase due to the minimization of the electrostatic double layer. But nanoparticle systems, especially inorganic ones, are on the other hand an attractive system for charge determination by AUC due to the following reasons: constant density in absence of hydration effects; solid bodies, and thus no significant excluded volume effects.

Therefore, the only parameters of influence on the sedimentation coefficient that can vary for nanoparticle systems are size, shape, hydration, and charge, the latter being an average for each particle. However, as the shape and hydration also influence the diffusion coefficient via the frictional ratio,[15] these parameters cancel out as well as the size, if Fl-FFF data free from charge effects could be combined with sedimentation coefficient distributions from AUC. Consequently, our future work will focus on this topic with the goal to simultaneously determine size and charge distributions of charged nanoparticles, which are not accessible using currently available methods and which is an important topic if the number of charged nanoparticle systems of interest is considered.

Acknowledgment. Financial support of the Max-Planck-Society and the Israel Science Foundation, founded by The Israel Academy of Science and Humanities, is gratefully acknowledged. We thank Antje Völkel for the skillfully performed AUC experiments.

LA0347051

(29) Harding, S. E. *Biophys. Chem.* **2001**, *93*, 87.
(30) Stigter, D. *J. Phys. Chem.* **1980**, *84*, 2758.
(31) Cölfen, H.; Antonietti, M. *Adv. Polym. Sci.* **2000**, *150*, 67.
(32) Hokputsa, S.; Jumel, K.; Alexander, C.; Harding, S. E. *Eur. Biophys. J.* **2003**, *32*, 450.
(33) Cölfen, H.; Völkel, A. *Eur. Biophys. J.* **2003**, *32*, 432.